Journal of Applied Computational Intelligence

eISSN: 3136-6937

Vol. 4, No. 2, April, 2026

Articulation Constrained Neural ODE Prediction of Container Truck Trailer Rear Corner Trajectories

Fausto Rizzo[1,*], Armando Sacco[1], Quirino Santoro[1,2]

[1] *Department of Information Engineering, University of Padova, Padova, 35131, Italy*

[2] *Faculty of Information Technology, University of Trento, Trento, 38122, Italy*

Received 19 January 2026; Revised 16 May 2026; Accepted 20 May 2026; Published 23 May 2026

Abstract

Accurate trailer boundary prediction is needed when container trucks negotiate confined terminal roads, where a plausible tractor path can still produce substantial rear corner displacement. This study develops a continuous time predictor that combines an articulated vehicle kinematic backbone, a learned articulation rate residual, and an explicit articulation angle constraint. A compact residual with fixed nonlinear features and a fitted linear readout is identified from 5,000 derivative observations, while a tangent cone projection suppresses outward angular motion at the admissible boundary. Predicted trailer poses are converted into rear corner trajectories through a rigid footprint transformation. A reproducible feasibility experiment evaluates 60 evaluation maneuvers over a five second horizon using three model variants with identical commanded motion. The constrained predictor obtains a mean rear corner displacement error of 0.0072 m, compared with 0.3678 m for the kinematic baseline and 0.1152 m for the unconstrained neural model. Its mean articulation error is 0.0371 degrees, and no sampled articulation bound violations occur under the tested numerical projection. Distributional diagnostics, six maneuver families, five initial angle perturbation amplitudes, and five integration steps distinguish model accuracy from boundary enforcement and numerical sensitivity. These results characterize the relationship between articulation feasibility and rear corner tracking accuracy under the evaluated operating conditions. The formulation provides an interpretable basis for subsequent identification with measured steering, articulation, and trailer corner observations, where uncertainty in geometry and vehicle inputs must also be addressed.

Keywords: Trailer Swept Trajectory, Articulation Angle Constraint, Neural Ordinary Differential Equation, Container Truck Kinematics, Rear Corner Prediction

1. Introduction

Studies of articulated heavy vehicles examine how tractor and trailer paths diverge during turning maneuvers [1]. Comparisons of geometric and multibody models show that tire lateral slip changes this off-tracking as speed, curvature, payload, and road friction vary [2]. Research on extendable semitrailers further links changes in trailer configuration to variations in maneuverability and directional performance [3]. Recent vehicle trajectory prediction reviews examine physical, probabilistic, and learned approaches to forecasting motion for autonomous driving [4]. At a tight junction, changes in steering angle can cause the tractor and trailer to follow different paths. These effects occur in the vicinity of container stacks, gate islands and transfer lanes, and their extent differs along the route. An effective predictor should relate a geometrically feasible articulation response to the displacement of the corner nearest the obstacle. The resulting engineering problem couples vehicle motion prediction, angular feasibility, and footprint reconstruction. Its

* Corresponding author: rizzo.fa@dei.unipd.it

http://dx.doi.org/10.68406/jaci.2026.vol4iss2no9:123-136

➢ This is an open access article under the CC BY-NC-SA 4.0 license (https://creativecommons.org/licenses/by/4.0/).

© Authors retain all copyrights.

interpretation depends on vehicle geometry and prediction horizon. Therefore, the selected prediction target should be the same in all stages of model construction and experiment.

Kinematic models provide an interpretable representation of this coupling through simplified vehicle motion relationships. Many low-speed trailer tracking models simplify steering bias and deviations between nominal and operating geometry. Learning methods can correct for systematic errors when the data cover the relevant operating range. As a result, sequence-based predictors have been used to estimate vehicle trajectories under different motion histories. Reasonable ranges of articulation should also be specified in addition to reproducing the recorded motion. The angular error is relatively small at the start of the forecast but increases significantly later on, thus altering the occupied boundary. This angular sensitivity motivates incorporating articulation information into the position-based training target. Enforcing an angular limit while retaining the nominal rate discrepancy can preserve feasibility while leaving substantial tracking error. The design problem is to combine an interpretable articulation equation with an adaptable correction mechanism while specifying the guarantee provided by the constraint. The constraint guarantees angular admissibility under the stated assumptions; collision avoidance requires separate clearance and uncertainty assessments. The engineering interpretation is also dependent on the particular point of measurement for spatial discrepancy and the time interval of forecast observation.

Continuous time learned dynamics provide a convenient representation when observation times, forecast intervals, and downstream sampling requirements differ. Neural ordinary differential equations represent a learned vector field evaluated through numerical integration [5]. Residual physics methods augment an analytical model with a learned correction that represents discrepancies between predicted and observed motion [6]. For a container truck, articulation is a useful location for such a correction because it directly connects tractor turning to trailer orientation. Constraint handling nevertheless requires care. A finite penalty can discourage angular violations while leaving them possible for an unfamiliar maneuver, whereas a projected vector field has a more explicit boundary interpretation. Numerical integration introduces a separate issue: preserving admissibility at intermediate stages requires explicit attention to the finite step update. Boesen et al. [7] incorporated auxiliary algebraic trajectory information into neural dynamics through projection and stabilization methods. This distinction is relevant to swept trajectory prediction because geometric errors can accumulate even when the articulation state remains within its prescribed interval. A defensible evaluation therefore needs separate measures of trajectory error, angular error, bound violations, and sensitivity to numerical resolution. Reporting these quantities separately makes the source of a favorable result easier to inspect.

To examine how articulation feasibility affects trailer boundary prediction, this study combines an explicit angular constraint with learned continuous time dynamics in a reproducible evaluation. The methodological contribution is the explicit separation of nominal articulation dynamics, learned rate correction, and boundary enforcement in a corner-oriented predictor; commanded tractor motion is held fixed across the principal comparisons. Surveys of multi-future trajectory prediction examine datasets and evaluation metrics alongside the accuracy and diversity of predicted motion [8]. The experimental scope is limited to forward motion with known future commands and one vehicle geometry; the reported evidence concerns the specified operating family. The paper contains six sections. Section 2 reviews articulated vehicle models, learned continuous dynamics, and footprint-oriented evaluation. Section 3 defines the geometry, target trajectories, and admissible articulation set. Section 4 develops the residual predictor, its identification procedure, and its numerical constraint enforcement. Section 5 presents the evaluation protocol, comparative errors, robustness tests, and numerical sensitivity analyses. Section 6 states the conclusions, limitations, and directions for measured vehicle validation. This organization keeps the model assumptions distinct from the evidence used to assess them and places the reported numerical findings within their actual experimental scope. It also preserves the connection between the chosen prediction target, the angular constraint, and the independent questions that a measured validation campaign would need to resolve.

2. Related Work

2.1. Articulated vehicle motion and swept geometry

Articulated vehicle prediction begins with a choice of reference point and a consistent definition of the articulation angle. Tractor rear axle, hitch, trailer axle, and trailer corner trajectories serve different purposes and require consistent geometric transformations when used together. Dynamic models of tractor-trailer wheeled robots incorporate wheel slip when describing vehicle motion and designing path-following controllers [9]. These geometric dependencies are central when predictions support clearance assessment. An error measured at an axle may understate the displacement of an overhanging corner, particularly when the angular component dominates the position error. Studies of semi-trailer steering compare fixed and steerable trailer wheels through their effects on swept path width in confined operating spaces [10]. A rectangular trailer model is useful for reproducible analysis, although flexible components and local protrusions require an extended footprint model. The present work therefore reports a rear corner tracking target and preserves the complete rectangular pose transformation. A complete swept envelope additionally requires the full footprint and interpolation between poses. This distinction preserves the angular prediction mechanism while allowing

subsequent refinement of vehicle geometry. Consistent corner identities and coordinate conventions also support direct comparisons across steering reversals and maneuvers approaching the articulation limit.

2.2. Learned continuous dynamics and constraint handling

Learned vehicle dynamics range from direct prediction of future coordinates to structured correction of a nominal differential model. Zhang et al. [11] combined kinematic and data-driven vehicle trajectory forecasts through Kalman filtering to exploit their complementary information. This comparison motivates retaining an interpretable physical component while assessing the specific mechanism assigned to a learned correction. Continuous time formulations also allow the same fitted vector field to be evaluated at different prediction sampling intervals. Neural ordinary differential equation research discusses the interaction between the learned field and the numerical solver used to propagate it [12]. A comparison between continuous and discrete models must therefore specify the solver, input interpolation, and supervision signal as integral parts of the prediction method. Constraint enforcement adds a requirement for state feasibility. Physics-constrained neural ordinary differential equations have also been developed for stiff chemical kinetics, incorporating conservation constraints into learned dynamics [13]. Uncertainty, noisy observations, and errors in prescribed physical limits require dedicated estimation and calibration procedures alongside these modeling approaches. For the articulation problem, a nominal angular limit is a modeling parameter that requires vehicle specific calibration. A constrained trajectory can still be inaccurate if the input commands or underlying geometry are inaccurate. The open issue addressed here is the separation of residual learning from boundary enforcement within a small, auditable predictor. Cross-domain constraint studies provide methodological context; vehicle-specific validation must establish the geometric and operational implications for articulated trucks.

2.3. Evaluation for boundary prediction

Trajectory evaluation often emphasizes average and final displacement errors, but a footprint sensitive application needs to identify which vehicle point those errors describe. Cross-perspective trajectory prediction studies evaluate models on both egocentric and top-down datasets, making observation context an explicit part of the assessment [14]. For articulated trucks, a useful evaluation distinguishes ordinary turning from cases approaching the admissible angular boundary. Reporting only a mean angle error can conceal excursions that matter to downstream geometric reconstruction. Robust trajectory prediction methods use structured fusion of heterogeneous information to improve resistance to noisy inputs [15]. The experiment developed here varies the initial angle while retaining identical commands, making its robustness claim deliberately narrow. Numerical refinement provides an additional diagnostic: step dependent predictions reveal the contribution of the solver to the apparent vehicle response. Open-source frameworks for learning unknown equations provide reusable implementations and worked examples across several classes of dynamical systems [16]. Such documentation clarifies the relationship between identification targets, reference trajectories, and evaluation conditions, allowing reported errors to be interpreted alongside the assumptions used in model fitting. The remaining gap is a compact experiment that connects an explicit angular boundary rule to corner trajectory accuracy while disclosing these sources of dependence.

3. Problem Formulation and Geometric Representation

3.1. State definition and operating assumptions

The vehicle consists of a tractor and a rigid semitrailer joined by a hitch located at the tractor rear axle. This on-axle hitch approximation removes the hitch-offset parameter; transfer to a tractor with an offset fifth wheel requires the corresponding offset-dependent kinematics. The tractor wheelbase is 3.8 m, the hitch to trailer axle distance is 8.0 m, and the trailer rear overhang is 3.0 m. The modeled trailer width is 2.5 m. These dimensions define the vehicle configuration used throughout the evaluation. A ground fixed planar coordinate system records east and north displacement. Tractor heading is measured counterclockwise from its east axis, and articulation is tractor heading minus trailer heading. Positive steering follows the same turning convention. The target task is conditional prediction: future speed and steering commands are supplied, together with the initial vehicle state. It is therefore distinct from behavioral forecasting, where future driver commands must also be estimated. Motion is forward, the ground is planar, and the nominal equations exclude tire slip and body roll. These assumptions delimit the interpretation of every reported corner trajectory. The following equation collects the state variables and their heading relationship.

$$\boldsymbol{q} = [x \quad y \quad \psi \quad \beta]^{\top}, \psi_t = \psi - \beta \tag{1}$$

In the state equation, the first two components locate the hitch, the third gives tractor heading, and the fourth gives articulation. Trailer heading is derived directly from tractor heading and articulation, preserving consistency between the two angular representations. The measured initialization may contain an articulation perturbation in the robustness experiment, but the main comparison uses the specified reference initial condition. Speed and steering are evaluated on a uniform grid, and the same input sequence is supplied to every model. This arrangement isolates the articulation

dynamics because tractor translation and yaw propagation remain shared. The resulting displacement errors consequently describe articulation prediction conditional on the supplied tractor motion. The forecast horizon captures the articulation response over a local maneuver segment. Forecast states are retained at every evaluation instant, allowing the angular history and reconstructed corners to be inspected together. Figure 1 describes the geometry and coordinate transformation as a single workflow, from initial state and commands through articulation prediction to trailer footprint coordinates.

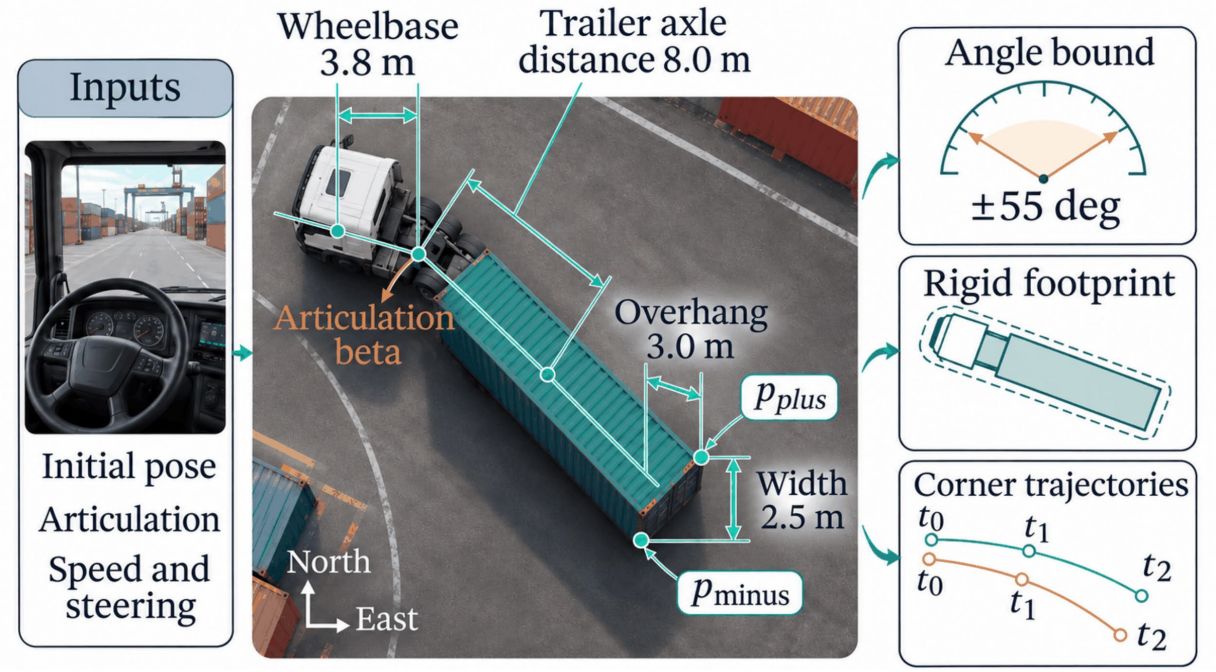


Figure 1. Geometry and prediction target workflow for an on axle articulated container truck

3.2. Nominal motion and rear corner reconstruction

The nominal motion model treats the tractor as a bicycle and the trailer axle as a rolling contact aligned with the trailer heading. The articulation rate is the difference between tractor yaw rate and trailer yaw rate. A compact representation is sufficient because the study learns a correction only for this relative rotation. The nominal model remains responsible for the translational components and for converting steering into tractor heading change. This allocation makes discrepancies in the learned articulation directly observable in the reconstructed trailer corner position and defines the scope of residual compensation. Tractor wheelbase errors and speed command bias require separate calibration to preserve the physical interpretation of the learned articulation correction. The nominal baseline therefore remains useful even when its tracking error is higher, since it reveals the behavior produced by geometry alone. Steering, articulation, and heading enter all trigonometric calculations in radians; articulation statistics and angular plot axes are converted to degrees for reporting. The nominal motion equation expresses tractor translation, tractor yaw, and articulation response as

$$\dot{x} = v\cos\psi, \quad \dot{y} = v\sin\psi,$$
$$\dot{\psi} = \frac{v\tan\delta}{L_c}, \quad \dot{\beta}_0 = \dot{\psi} - \frac{v\sin\beta}{L_t}. \tag{2}$$

With the two signs identifying the rear corners, the footprint equation becomes

$$\boldsymbol{p}_{\pm} = \begin{bmatrix} x \\ y \end{bmatrix} - (L_t + l_r)\begin{bmatrix} \cos\psi_t \\ \sin\psi_t \end{bmatrix} \pm \frac{w}{2}\begin{bmatrix} -\sin\psi_t \\ \cos\psi_t \end{bmatrix}. \tag{3}$$

The rear corners are reconstructed from the hitch position using trailer heading, axle spacing, overhang, and half width. The transformation is deterministic, so the reported corner error directly reflects the propagated pose difference under the shared geometry. The evaluation tracks the corner obtained with the positive trailer normal, while the saved trajectory record contains both rear corners. The reported error therefore applies to one consistently identified corner; conclusions about the opposite corner or the full footprint require their own spatial error measures. The footprint transformation also identifies the route to a fuller occupied region estimate: front corners can be appended using a specified trailer front extent, and successive rectangles can be combined spatially. Those operations require explicit sampling and interpolation rules before the reconstructed footprint can support continuous clearance assessment. A rear corner trajectory is a boundary relevant prediction target, but an exact swept region requires more than the single corner

metric. This distinction is especially important when a downstream planner uses the output near a narrow obstacle boundary.

3.3. Admissibility and prediction targets

The range of permissible articulation is symmetrical around the straight-line position, and in this study, it is set to 55 degrees. This bound defines the admissible articulation interval; the mechanical jackknife threshold requires vehicle-specific calibration. The selected interval is a configured model limit rather than a measured universal jackknife threshold; mechanical stops, operating policies, and hose clearance require vehicle-specific calibration. The prediction target is an angle and the coordinates of the rear corner at the predicted time. Mean corner displacement is the average spatial difference; final corner displacement is at the end of the prediction window; high percentiles show distribution tails. Mean absolute articulation error provides an internal state diagnostic, and the proportion of samples outside the specified range shows numerical feasibility. These measures characterize distinct aspects of geometric accuracy and state feasibility. Collision probability, sampled feasibility and tracking accuracy are all different metrics. They are kept separate so that the effect of residual identification and the effect of the hard-boundary rule can be evaluated independently. The formulation provides an extension point for uncertain geometry and stochastic inputs, while the present comparison holds these factors fixed. The saved trajectories retain both rear corners, allowing alternative spatial metrics to be evaluated using the fitted model.

4. Articulation Constrained Neural ODE Method

4.1. Residual vector field and identification

The proposed predictor adds a scalar neural residual to the nominal articulation rate. Its inputs are normalized articulation, speed, and steering. Their scaling uses the prescribed angular bound, a reference speed of 4 m per second, and a reference steering magnitude of 0.45 radians. The feature layer contains 24 hyperbolic tangent units with fixed random weights and biases. A constant and the three normalized inputs are appended to these nonlinear features, yielding 28 coefficients in the trained readout. The model is a neural ordinary differential equation whose vector field uses fixed random nonlinear features and an optimized linear readout; only the 28 readout coefficients are identified. The distinction matters because the experiment tests whether a small identifiable residual is sufficient for the reference rate discrepancy. Training uses derivative supervision at independently sampled operating points. Each target combines the reference residual rate with a small independent Gaussian perturbation, providing controlled derivative supervision. This makes the identification problem controlled and comparatively favorable, and it limits direct transfer of the reported performance to field data. A residual equation couples the nominal angular rate to the nonlinear feature readout:

$$f_\theta(\beta, v, \delta) = \dot{\beta}_0 + \boldsymbol{\theta}^\top \boldsymbol{\phi}(\beta, v, \delta)$$
$$\phi = \begin{bmatrix} 1 \\ \boldsymbol{u} \\ tanh(\boldsymbol{W}\boldsymbol{u} + \boldsymbol{b}) \end{bmatrix}. \tag{4}$$

The reference residual combines a saturating articulation term, a steering dependent term scaled by speed, and a bilinear articulation speed term. Their coefficients are disclosed in the accompanying code so that the reference rate formulation can be inspected directly. Identification draws 5,000 operating points uniformly over the specified ranges and adds rate noise with a standard deviation of 0.001 radians per second. The readout is obtained by regularized least squares with a ridge parameter of 0.001. Only this readout is optimized; random features remain fixed after initialization. The training objective therefore has a direct numerical solution, providing a deterministic readout estimate. The reported random seed fixes feature initialization, sampled identification points, and derivative noise for this fitted model; variation across independent fits remains unquantified. Releasing these details also reveals a methodological dependency: the training targets and rollout reference share the same reference residual function. Independent test maneuvers prevent reuse of identical state sequences, but the comparison retains a shared reference dynamics formulation. The experiment is an internal feasibility assessment of identification and constraint handling.

4.2. Angular boundary projection

The constrained model projects its scalar rate onto the tangent directions allowed by the articulation interval. Inside the interval the learned rate remains unchanged. At the positive boundary, a positive rate is suppressed; at the negative boundary, a negative rate is suppressed. A rate pointing back toward the interval is retained. The projection is directional, retaining the inward response when steering changes after boundary contact. This behavior is useful for steering reversals because the trailer must be allowed to return toward straight alignment. The theoretical admissibility statement assumes a feasible initial angle, a correctly specified interval, and the ideal projected differential evolution. Observations outside that interval require a separate initialization and estimation policy. The applied offsets in the perturbation experiment

remain within the feasible initial range. The shared residual coefficients isolate the effect of projection from changes in identification parameters. Boundary behavior is specified through the projected rate equation below.

$$\dot{\beta} = \Pi_{T(\beta)} f_\theta, \beta \in [-B, B], \quad \Pi_{T(B)} f = min(f, 0), \Pi_{T(-B)} f = max(f, 0). \tag{5}$$

A finite step can cross the boundary even when the projected field is correctly defined at its endpoints. The implementation consequently clips the accepted articulation state after each integration step. This practical safeguard makes the sampled violation result partly an implementation property, and that fact is stated explicitly when interpreting the experiment. Continuous projection specifies allowable boundary motion, while accepted state clipping preserves the finite step output range. Intermediate Runge Kutta stage values can still leave the interval before acceptance. The step sensitivity test measures the combined effect of finite-step propagation and input holding on accepted trajectories; it does not isolate intermediate-stage excursions. Figure 2 presents the full identification and inference workflow, including the split between derivative supervised fitting and projected rollout. The same fitted coefficients feed the unconstrained and constrained neural variants, so their performance difference can be attributed to the boundary treatment under the stated experiment.

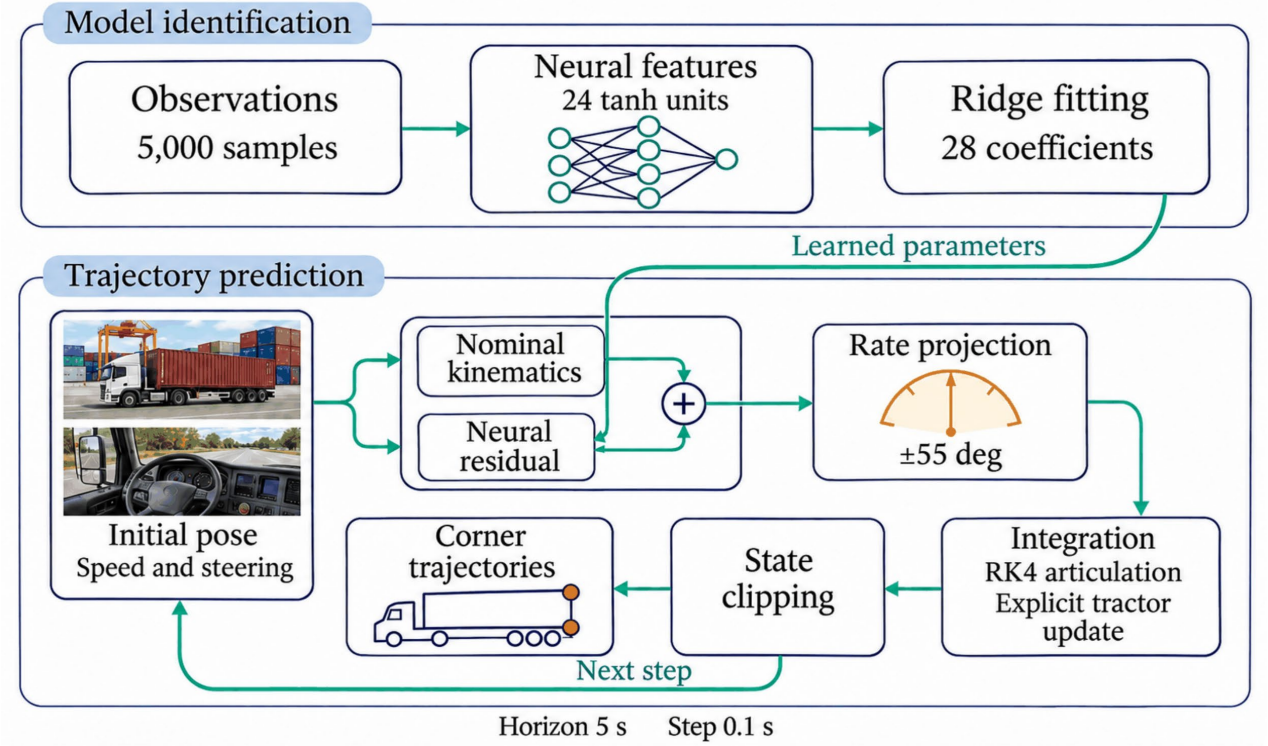


Figure 2. Identification and inference workflow for the articulation constrained neural ODE

4.3. Integration and comparative evaluation

Articulation is propagated with classical fourth order Runge Kutta at the main step of 0.1 seconds. Tractor translation and heading use the shared explicit update in the released implementation. The coupled rollout consequently retains the order limitation of the shared explicit tractor update. Speed and steering are evaluated at the beginning of the step and held constant within the articulation stages. This input handling is identical across the three principal models, allowing a focused comparison but leaving a discretization effect that matters when the step is changed. The angular clipping occurs after the accepted update. Corner positions are then reconstructed from the stored pose. The reference rollout uses the disclosed truth residual and the same accepted state bound treatment at the primary resolution. Consequently, the principal errors measure agreement with the discretized reference experiment at the primary resolution. The separate fine resolution comparison examines this numerical dependence for one designated maneuver. For spatial evaluation, the error equation relates instantaneous corner displacement to its average and final horizon measures.

$$e_i = \|\hat{\boldsymbol{p}}_i - \boldsymbol{p}_i\|_2, \quad ADE = mean_i e_i, FDE = mean_k e_{k,\,final}. \tag{6}$$

Mean corner error averages pointwise Euclidean distances over retained instants and then over the 60 maneuvers; final corner error averages the endpoint distances over those maneuvers. Angular errors are converted to degrees before aggregation. A bound violation is recorded only when the magnitude exceeds the prescribed interval by more than a

small floating-point tolerance. The kinematic baseline propagates the nominal unconstrained articulation dynamics. The unconstrained neural model propagates the same learned readout as the proposed model through an unrestricted articulation update. The three variants compare residual correction and boundary treatment within the implemented design; a projected kinematic baseline is still needed to estimate their interaction in a complete factorial ablation. The implemented comparisons focus on the nominal, residual, and constrained residual variants under identical inputs. Computational assessment uses integration interval counts, with hardware latency reserved for a measured benchmark. The numerical experiment instead reports integration interval counts and step dependent corner differences, keeping computational evidence within the quantities evaluated by the accompanying implementation.

5. Experiments and Analysis

5.1. Experimental protocol and trajectory behavior

The evaluation protocol separates derivative identification from maneuver rollout. The training set contains 5,000 observations sampled across articulation magnitudes up to 55 degrees, forward speeds of 0.5–4.0 m per second, and steering angles of minus to plus 0.45 radians. Table 1 specifies the geometry, rate noise, regularization, and numerical settings. Out-of-distribution trajectory prediction benchmarks introduce explicit scene shifts to evaluate transfer beyond the training distribution [17]. For the within-family comparison used here, the 60 evaluation identifiers supply command histories that differ from the sampled identification points while retaining the same reference dynamics formulation. Each trajectory contains 51 retained states over five seconds, including the initial state; the maneuver identifiers represent different command histories within the same reference dynamics family. Six command families provide ten maneuvers each, with sustained steering in one family and phase shifted sinusoidal steering in the remaining families. Intention-aware trajectory forecasting incorporates driver maneuvers and surrounding vehicle interactions into predictions of future motion [18]. Here, future speed and steering commands are supplied to isolate articulation dynamics: all model variants receive identical input sequences, and their tractor motion is propagated through the same numerical update. The resulting comparison attributes corner displacement differences to articulation prediction under fixed geometry. It establishes an identification experiment within a specified motion family, with transfer to measured terminal operations reserved for subsequent validation.

Table 1. Vehicle geometry and experimental protocol

Item	Value
Tractor wheelbase / trailer axle spacing	3.8 m / 8.0 m
Rear overhang / width	3.0 m / 2.5 m
Articulation magnitude bound	55 degrees
Training points / readout coefficients	5,000 / 28
Training speed / steering ranges	0.5–4.0 m/s / ±0.45 rad
Derivative noise / ridge parameter	0.001 rad/s / 0.001
Test maneuvers / horizon / main step	60 / 5 s / 0.1 s
Random seed	20261112

Figure 3(a) presents maneuver 0, which begins at a 43-degree articulation and applies a sustained 0.44 radian steering command. Its constrained final corner error rounds to 0.0000 m at the reported precision under the shared tractor motion and boundary treatment. The reference and constrained paths approach the same configured angular boundary, whereas the unrestricted models continue to accumulate an orientation discrepancy. This case isolates the boundary mechanism because steering maintains the outward angular tendency after the initial turn. Figure 3(b) presents maneuver 17, whose varying steering produces a constrained final corner error of 0.0166 m. Here, the separation between the nominal and learned paths reflects residual identification over the changing articulation history. Path-following studies of articulated vehicles assess turning performance through quantities such as swept path width and trailer cut-in [19]. In the present geometry, the trailer rear-edge midpoint lies 11 m longitudinally behind the hitch, providing a direct geometric explanation for the visible separation between the corner paths. One second markers distinguish the temporal progression from the apparent curvature of each trajectory. The comparison between these two maneuvers also separates an error removed by angular saturation from an error reduced through residual learning. Axis values define spatial displacement; the fixed plotting box ratio provides consistent panel sizing across the figure set.

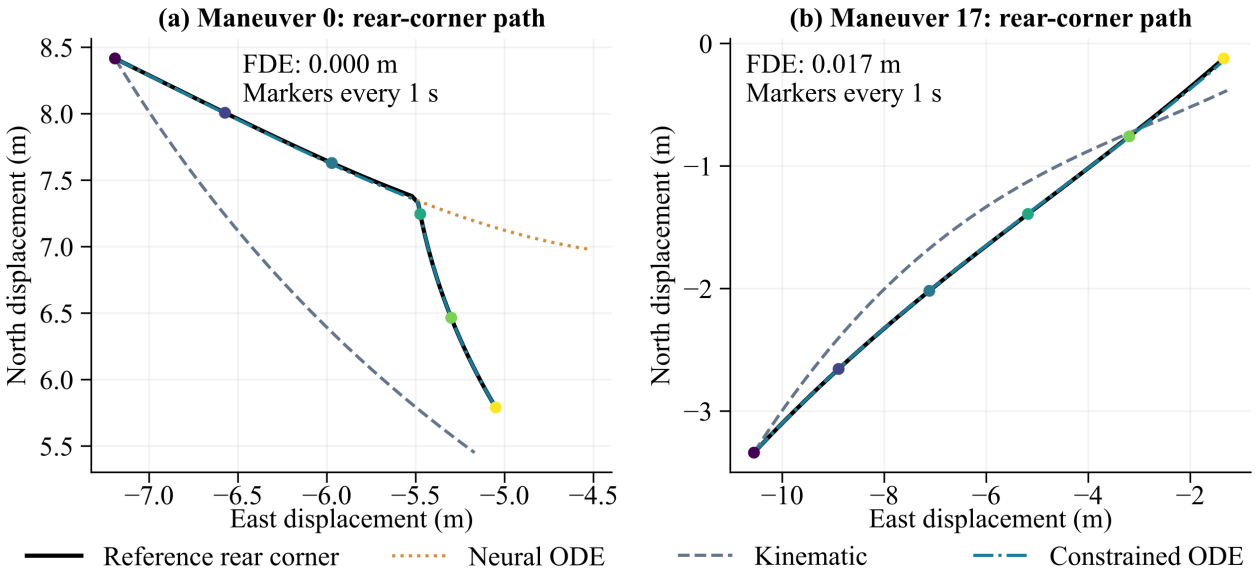


Figure 3. Representative predicted rear corner trajectories. (a) Sustained steering maneuver 0. (b) Varying steering maneuver 17

Table 2 reports a constrained mean corner error of 0.0072 m, compared with 0.3678 m for the kinematic baseline and 0.1152 m for the unconstrained neural variant. The decrease relative to the kinematic model is 98.05 percent within this evaluation protocol, corresponding to an absolute reduction of 0.3606 m based on the displayed means. Its final error is 0.0109 m and pooled 95th percentile error is 0.0226 m. These statistics describe different portions of the forecast: the final error emphasizes accumulated displacement, whereas the pooled percentile combines the 3,060 retained state samples from the 60 trajectories and therefore includes temporal dependence within maneuvers. Trajectory prediction assessments report average and final displacement errors alongside qualitative trajectory comparisons to examine aggregate accuracy and individual prediction behavior [20].

Table 2. Comparative errors and sampled angular feasibility on the evaluation maneuver set

Model	ADE m	FDE m	P95 m	Angle MAE deg	Violations %
Kinematic	0.3678	0.6097	0.9626	1.9038	4.2157
Neural ODE	0.1152	0.3565	1.0354	0.5966	9.1503
Constrained ODE	0.0072	0.0109	0.0226	0.0371	0.0000

Figure 4(a) therefore displays per maneuver mean errors, revealing the spread concealed by the pooled average. Its upper tail indicates whether a model's mean performance is accompanied by a small group of difficult trajectories.

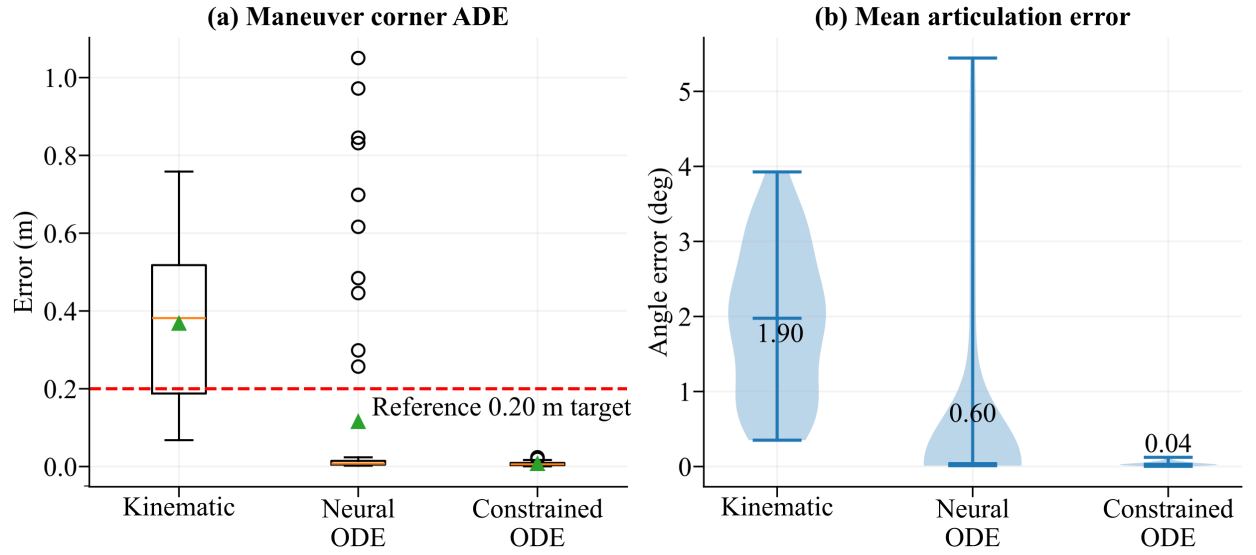


Figure 4. Distributions of maneuver level errors. (a) Rear corner average displacement error with mean indicators and a reference 0.20 m target. (b) Mean absolute articulation error with median indicators and numerical mean annotations

Figure 4(b) shows the corresponding articulation error distributions, with a constrained mean of 0.0371 degrees. The angular and spatial distributions can be read together because the geometry and tractor inputs are shared. Their joint reduction is consistent with a more accurate trailer orientation history. The reference 0.20 m line is an analyst-selected visual comparison target rather than an independently validated operational tolerance; selecting an operational threshold would additionally require obstacle geometry, sensing uncertainty, and vehicle specific clearance requirements.

5.2. Constraint effects and sensitivity to initial observations

The constraint diagnostics examine angular feasibility alongside corner trajectory accuracy. Figure 5(a) relates maneuver mean corner error to maximum reference articulation, allowing errors near the configured angular limit to be compared with those from moderate turning. The unconstrained neural model retains a small central error population while exhibiting larger errors among trajectories driven toward the boundary. Figure 5(b) exposes this structure through the empirical distribution: its central mass and upper tail occupy different error ranges. The pooled 95th percentile of the unconstrained neural model is 1.0354 m, exceeding the kinematic model's 0.9626 m despite its lower mean error. This contrast indicates that learning the residual alone improves many trajectories while leaving a boundary sensitive failure mode. Experimental work on articulated dump trucks uses scenario-specific kinematic models to improve path tracking in forward and reverse operation [21]. The present comparison examines angular admissibility separately from corner tracking error. Figure 5(c) reports violation fractions of 4.22, 9.15, and 0.00 percent for the kinematic, unconstrained neural, and constrained neural models. Accepted state clipping directly explains the constrained sampled feasibility result. Figure 5(d) displays error histories for six selected identifiers and reveals when disagreement develops or is reduced during propagation. The combination of a distribution, a feasibility count, and time resolved errors distinguishes a broadly accurate interior response from behavior governed by the prescribed angular boundary.

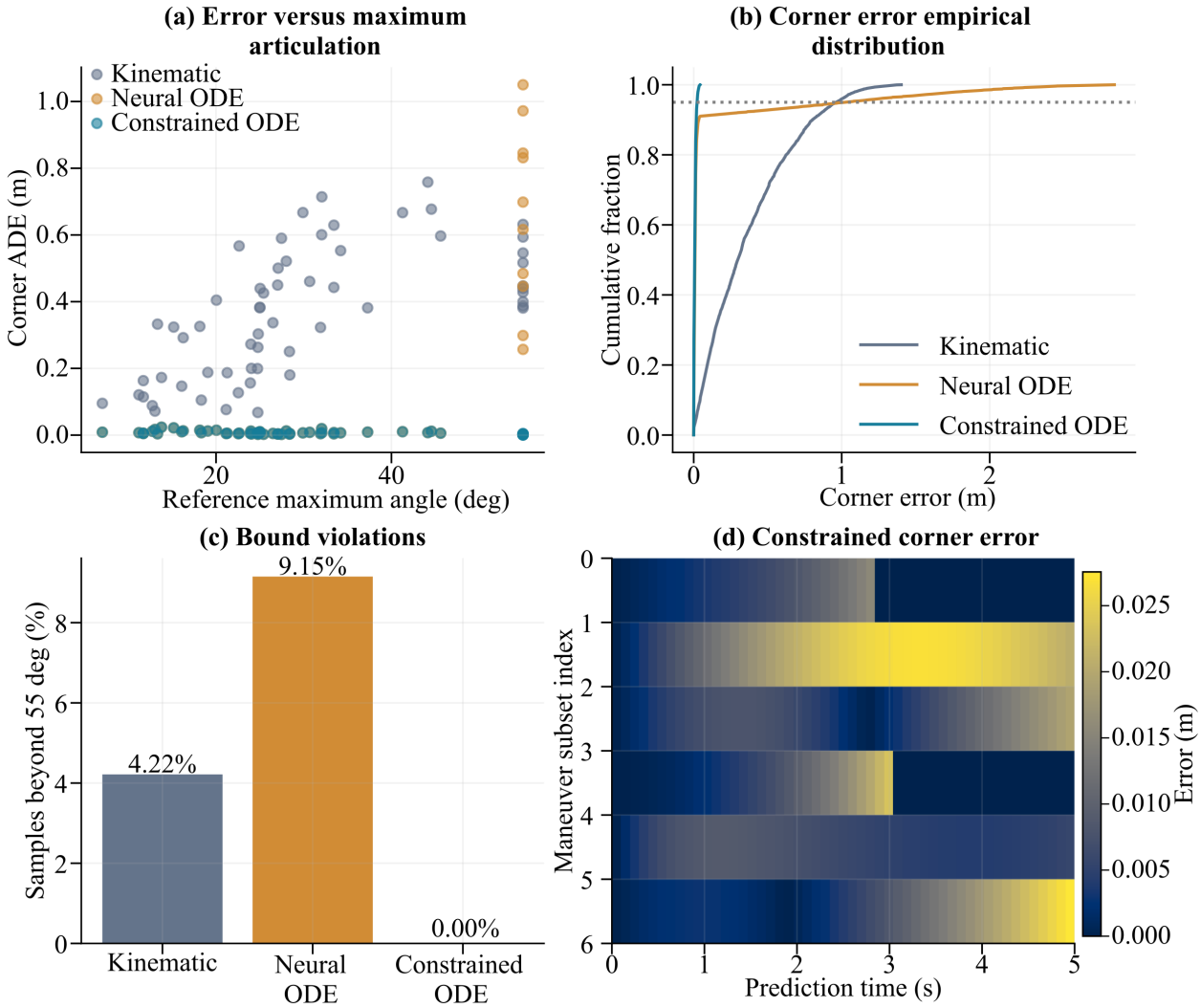


Figure 5. Accuracy and articulation feasibility diagnostics. (a) Mean corner error versus maximum reference articulation. (b) Pooled corner error empirical distributions. (c) Fractions of sampled states beyond the 55-degree interval. (d) Constrained error histories for maneuver identifiers 0, 10, 20, 30, 40, and 50.

The initialization test examines changes in corner error across a prescribed range of articulation offsets. The present test applies signed articulation offsets with maximum amplitudes of 0, 0.5, 1, 2, and 3 degrees; a deterministic sinusoidal factor assigns the offset for each identifier. Figure 6(a) compares the resulting mean corner errors across the three models. For the constrained predictor, these errors are 0.0072, 0.0385, 0.0761, 0.1518, and 0.2275 m, respectively. The increasing displacement reflects the propagation of an initially rotated trailer footprint through otherwise identical future commands. Figure 6(b) places the same five operating points against a reference 0.20 m target, making the crossing between the two largest tested amplitudes visible. The grouped columns emphasize differences between models at each amplitude, while the scatter view emphasizes the response to the imposed observation error. At three degrees, the kinematic and unconstrained neural variants record 0.4321 and 0.3393 m, respectively. Their different starting errors and subsequent changes show that robustness should be interpreted alongside nominal accuracy. Risk-aware stochastic vehicle predictors represent uncertain future motion through probabilistic forecasts with spatial and temporal interaction modeling [22]. The displayed amplitudes are deterministic maximum offsets, not standard deviations or confidence bounds; the observed crossing applies to this signed-offset protocol. A probabilistic sensor tolerance would require a measured observation error model and a separately defined coverage criterion.

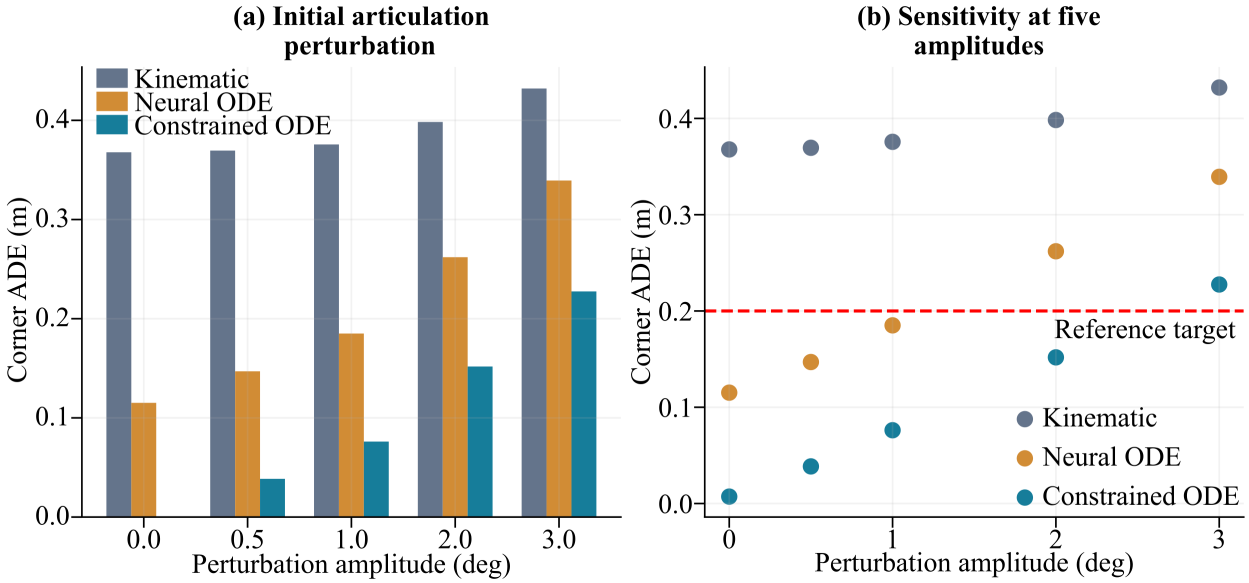


Figure 6. Response to five initial articulation perturbation amplitudes. (a) Grouped column comparison of mean corner error for three models. (b) Sensitivity scatter plot with a 0.20 m reference threshold.

The open-loop test propagates an imposed initial articulation offset through the angular dynamics and footprint transformation without subsequent observation updates. The largest amplitude increases constrained mean corner error by approximately 0.2203 m relative to its nominal value, showing that boundary enforcement leaves substantial sensitivity to feasible initial angle errors. Its directional behavior helps explain this outcome. Near the positive limit, an outward perturbation may be reduced when the accepted state reaches the bound, whereas an inward perturbation can persist until the dynamics move the trailer back toward it. Steering reversals can alter this relation by changing the direction of angular motion during the forecast. Articulated vehicle state estimators combine dynamic models with extended or unscented Kalman filtering to estimate sideslip angle and yaw rate [23]. Geometry introduces another identifiable source of sensitivity: an incorrect axle distance affects both trailer yaw rate and the lever arm used for corner reconstruction. Since this test holds geometry fixed, it isolates the observation channel while retaining the angular boundary mechanism. A measured calibration study should consequently evaluate bias direction, boundary proximity, and steering history together when determining the initialization accuracy needed for a specified corner error target.

5.3. Maneuver heterogeneity and numerical resolution

The family and horizon diagnostics examine where tracking error varies across command histories and forecast times. Figure 7(a) separates constrained corner errors into six control families, each containing ten identifiers. The differing violin widths and medians describe the interaction between phase, steering amplitude, and boundary contact within the evaluation set. Figure 7(b) displays errors at horizons of 1, 2, 3, 4, and 5 seconds, preserving the spread across maneuvers at each time. The upper observations increase with the prediction interval, while several trajectories retain small errors after reaching the shared angular limit. These tracking diagnostics characterize the geometric component of a broader safety assessment. Logged-trajectory safety evaluations examine whether risk metrics provide warnings before a vehicle enters a collision-unavoidable situation [24]. Applying such a criterion would additionally require obstacle motion and a defined collision test. Figure 7(c) relates articulation error to corner error and uses color to identify forecast time. The

near linear association is consistent with the fixed rear corner lever arm over the observed angular error range. Figure 7(d) compares final corner error distributions for the three models using 60 endpoints per curve. Its tail emphasizes the accumulated displacement of boundary sensitive maneuvers, complementing the pooled distribution shown earlier. These complementary views locate heterogeneity in control family, forecast duration, and angular state. The family labels describe specified command patterns, providing a reproducible basis for selecting difficult trajectories for subsequent measured vehicle testing.

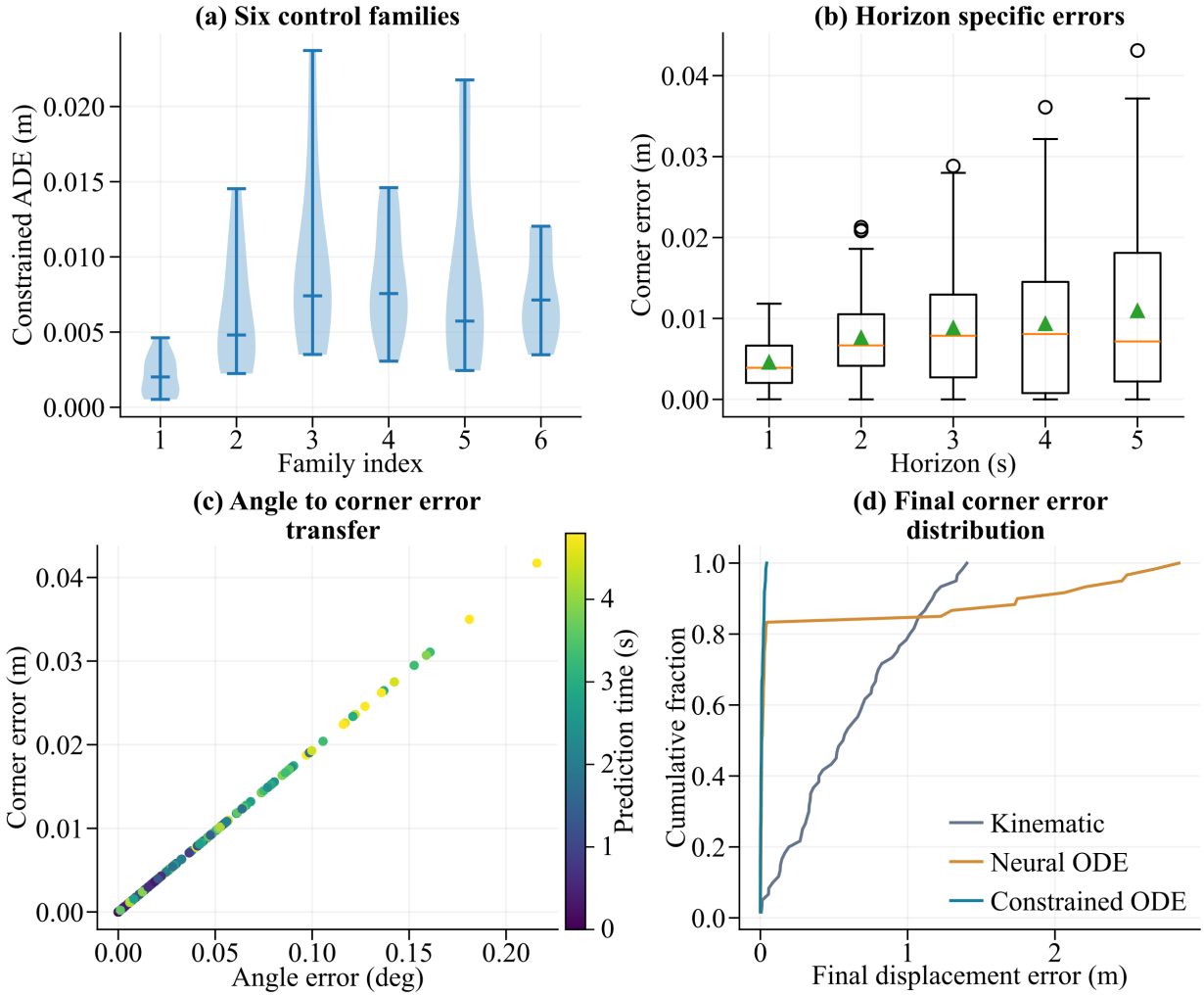


Figure 7. Maneuver and horizon dependence. (a) Violin plots for six command families. (b) Constrained corner error at five horizons. (c) Articulation error versus corner error, colored by prediction time. (d) Final corner error distributions for all model variants.

The integration step test examines the sensitivity of the reconstructed corner endpoint to numerical resolution. Figure 8 evaluates maneuver 17 at integration steps of 0.05, 0.10, 0.20, 0.25, and 0.50 seconds, corresponding to 100, 50, 25, 20, and 10 intervals over the forecast. Relative to a 0.025 second constrained reference, the final corner differences are 0.0252, 0.0751, 0.1728, 0.2206, and 0.4487 m. The primary step therefore produces a difference approximately three times that observed at 0.05 seconds. This sensitivity is materially larger than the constrained model's mean discrepancy against the reference evaluated at the primary resolution. Analysis of neural ordinary differential equation training identifies solver-dependent oscillations in automatically differentiated gradients and develops numerical corrections [25]. The refinement experiment here examines numerical sensitivity during forward propagation. The fine-step reference is a numerical comparator rather than an exact continuous-time solution. The two comparisons measure different quantities: shared resolution agreement isolates the fitted articulation field, whereas refinement changes tractor propagation and command holding as well as angular integration. The approximately sixfold increase between the primary and coarsest step indicates a practical accuracy cost when interval count is reduced. The 0.05 m guide is crossed between the two finest tested steps for this maneuver. Interval counts provide an implementation independent workload descriptor; measured latency would additionally depend on hardware, batching, and software overhead.

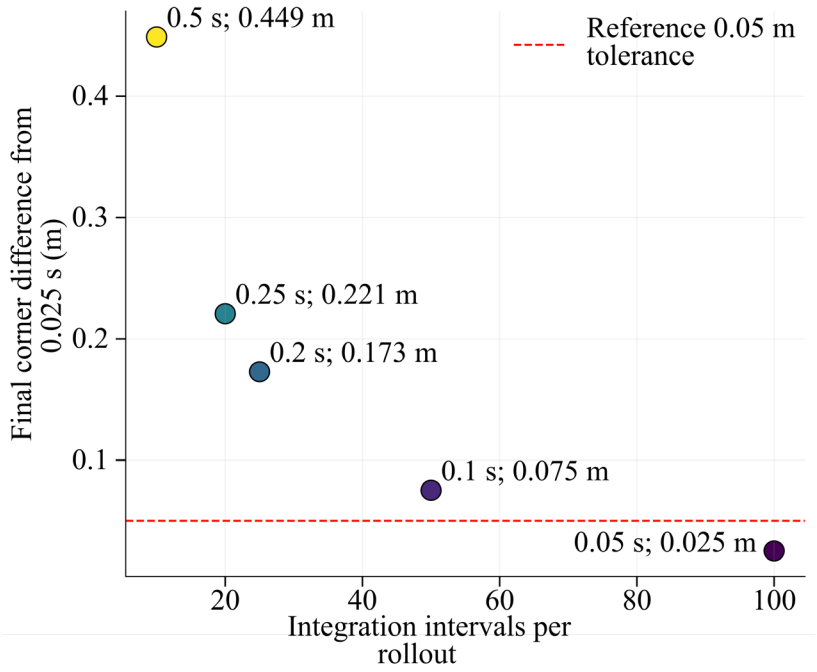


Figure 8. Numerical resolution sensitivity

The shared residual function and angular interval create a specific dependence in this experiment: approaching the boundary can reduce the difference between two previously distinct articulation histories. Reference trajectories occupy the prescribed boundary at 9.0850 percent of retained time samples. Within the sustained steering family, every constrained trajectory reaches the same final articulation as its reference, producing zero final corner displacement under the shared tractor motion. Its mean error over the complete horizon remains 0.0021 m because discrepancies develop before saturation. This distinction explains how a favorable endpoint can coexist with an earlier tracking error. Across the remaining families, constrained mean corner errors are 0.0064, 0.0098, 0.0084, 0.0087, and 0.0076 m. The largest family mean occurs under a varying command history, where the angular state spends more of the forecast responding within the interval. Comparative studies of learned temporal dynamics examine how rollout strategy, sampling configuration, and prediction horizon affect the balance between accuracy and stability [26]. These values also clarify the numerical comparison: agreement after clipping can reduce endpoint disagreement, while errors in the explicitly propagated tractor position persist in the reconstructed corner coordinates. The fine step comparison retains that positional contribution even when the articulation state approaches the same configured limit.

6. Conclusion

This paper developed an articulation-constrained neural ordinary differential equation model for predicting container truck trailer corner trajectories. The model retains an interpretable articulated-vehicle kinematic backbone and learns a compact correction to the articulation rate. Tangent cone projection defines admissible angular motion, while accepted-state clipping preserves the configured interval during numerical rollout. A rigid-footprint transformation connects the predicted pose to the trailer rear corners. Separate experiments were conducted to investigate the impact of nominal geometry, residual identification and angular boundary treatment. Distributional, maneuver-specific, perturbation and numerical refinement diagnostics related the internal-state behavior to the spatial prediction objective.

The evaluation covers a fixed reference dynamics family and a prescribed set of predictor inputs. Direct derivative supervision simplifies identification relative to estimating derivatives from noisy measured trajectories, and the shared reference mechanism limits the independence of the present validation. Shared future commands remove behavioral uncertainty, while the fixed geometry excludes variation between vehicles. The sampled feasibility results reflect both the numerical clipping rule and the projected field. A continuous occupied region requires full footprint reconstruction, temporal interpolation, and a separate collision assessment. Broader operational validation requires additional vehicle configurations, independently characterized inputs, and terminal layouts.

Future research should first identify the residual from synchronized steering, speed, articulation, and pose measurements, then evaluate it on held-out trucks and terminal layouts. The state estimator should address articulation bias, intermittent observations, and sensor delay before prediction. The geometric representation should be extended to a complete swept boundary with explicit treatment of interpolation and uncertain dimensions. Further research should examine reverse maneuvers and uncertainty in the prescribed angular limits. Comparisons of alternative neural architectures under the same loss function and data conditions should assess their effect on generalization. Independent

numerical experiments and measured latencies should support separate assessments of model accuracy and computational performance.

7. Declarations

7.1 Author Contributions

Fausto Rizzo contributes to conceptualization, methodology, software, validation, analysis, investigation, data collection, draft preparation, manuscript editing, visualization, supervision, project administration, and funding acquisition. Armando Sacco contributes to validation, analysis, investigation, data collection, draft preparation. Quirino Santoro contributes to conceptualization, validation, analysis. All authors have read and agreed with the manuscript before its submission and publication.

7.2 Funding and Acknowledgments

This research received no specific financial support from any funding agency.

7.3 Institutional Review Board Statement

Not applicable.

7.4 Informed Consent Statement

Not applicable.

7.5 Date Availability

Not applicable.

7.6 Declaration of Competing Interest

The authors declare that they have no known competing financial interests or personal relationships that could have appeared to influence the work reported in this paper.

7.7 Declaration of generative AI and AI-assisted technologies

During the preparation of this manuscript, the authors utilized Grammarly for linguistic polishing, logical organization and draft revision. The generative AI tool was not involved in research design, data collection, data analysis, or the equation of core conclusions. All outputs generated by AI were reviewed, revised and verified manually by the authors. The authors take full responsibility for all content of this manuscript.

8. References

[1] Ghandriz, T., Jacobson, B., Nilsson, P., & Laine, L. (2024). Trajectory-following and off-tracking minimisation of long combination vehicles: A comparison between nonlinear and linear model predictive control. Vehicle System Dynamics, 62(2), 277–310.https://doi.org/10.1080/00423114.2022.2164513

[2] Neighborgall, C., Chen, Y., & Ahmadian, M. (2024). Tyre lateral slip effect on off-tracking of a long combination vehicle. Vehicle System Dynamics, 62(11), 2765–2784. https://doi.org/10.1080/00423114.2024.2304052

[3] Zhou, Q., Zhang, H., He, Y., Su, Y., Jiang, Y., & Zheng, S. (2025). A directional-performance control design for articulated heavy vehicles with extendable-trailers. Vehicle System Dynamics, 63(12), 2393–2438. https://doi.org/10.1080/00423114.2024.2419460

[4] Yan, Y., Zhang, P., Du, C., Wang, H., Wang, H., Pi, D., & Chen, Y.-H. (2026). Vehicle trajectory prediction for autonomous driving applications: State-of-the-art review, research challenges, and future directions. Automotive Innovation, 9(2), 263–295. https://doi.org/10.1007/s42154-025-00382-8

[5] Lehtimäki, M., Paunonen, L., & Linne, M.-L. (2024). Accelerating neural ODEs using model order reduction. IEEE Transactions on Neural Networks and Learning Systems, 35(1), 519–531. https://doi.org/10.1109/TNNLS.2022.3175757

[6] Gao, J., Michelis, M. Y., Spielberg, A., & Katzschmann, R. K. (2024). Sim-to-real of soft robots with learned residual physics. IEEE Robotics and Automation Letters, 9(10), 8523–8530. https://doi.org/10.1109/LRA.2024.3446287

[7] Boesen, T., Haber, E., & Ascher, U. M. (2025). Neural DAEs: Constrained neural networks. SIAM Journal on Scientific Computing, 47(2), C291–C312. https://doi.org/10.1137/23M1574051

[8] Huang, R., Xue, H., Pagnucco, M., Salim, F. D., & Song, Y. (2025). Vision-based multi-future trajectory prediction: A survey.

IEEE Transactions on Neural Networks and Learning Systems, 36(8), 13691–13708. https://doi.org/10.1109/TNNLS.2025.3550350

[9] Babaei Robat, A., Arezoo, K., Alipour, K., & Tarvirdizadeh, B. (2024). Dynamics modeling and path following controller of tractor-trailer-wheeled robots considering wheels slip. ISA Transactions, 148, 45–63. https://doi.org/10.1016/j.isatra.2024.03.004

[10] Luu, D. L., Tran, X. D., Dinh, T. C. T., Thai, P. Q., & Truyen, P. H. (2025). Method for improving the maneuverability of the steering system for semi-trailer trucks. The University of Danang - Journal of Science and Technology, 23(9C), 69–73. https://doi.org/10.31130/ud-jst.2025.23(9C).537E

[11] Zhang, B., Yu, W., Jia, Y., Huang, J., Yang, D., & Zhong, Z. (2024). Predicting vehicle trajectory via combination of model-based and data-driven methods using Kalman filter. Proceedings of the Institution of Mechanical Engineers, Part D: Journal of Automobile Engineering, 238(8), 2437–2450. https://doi.org/10.1177/09544070231161846

[12] Zhu, A., Bertalan, T., Zhu, B., Tang, Y., & Kevrekidis, I. G. (2024). Implementation and (inverse modified) error analysis for implicitly templated ODE-nets. SIAM Journal on Applied Dynamical Systems, 23(4), 2643–2669. https://doi.org/10.1137/23M1564596

[13] Kumar, T., Kumar, A., & Pal, P. (2025). A physics-constrained neural ordinary differential equations approach for robust learning of stiff chemical kinetics. Combustion Theory and Modelling, 29(3), 332–347. https://doi.org/10.1080/13647830.2025.2478266

[14] Astuti, L., & Lin, Y.-C. (2025). ABi-LSTM: Attention-based bidirectional-LSTM for multiclass traffic agents trajectory prediction. IEEE Transactions on Vehicular Technology, 74(10), 15603–15618. https://doi.org/10.1109/TVT.2025.3572329

[15] Wang, X., Yang, D., Li, L., Li, C., Lian, J., Zhao, J., Zhang, Z., & Bian, Y. (2026). Robust trajectory prediction based on efficient fusion of heterogeneous information. IEEE Transactions on Vehicular Technology, 75(1), 114–129. https://doi.org/10.1109/TVT.2025.3591243

[16] Chen, J., Wu, K., & Xiu, D. (2025). DUE: A deep learning framework and library for modeling unknown equations. SIAM Review, 67(4), 873–902. https://doi.org/10.1137/24M1671827

[17] Ye, L., Zhou, Z., Wang, J., Li, Y.-H., Jan, N.-Y., Lin, Y.-R., & Lin, Y.-C. (2024). IMGTP: A unified framework for improving and measuring the generalizability of trajectory prediction models. IEEE Transactions on Intelligent Vehicles, 9(10), 6217–6231. https://doi.org/10.1109/TIV.2024.3364714

[18] Hasan, F., & Huang, H. (2024). Driver intention and interaction-aware trajectory forecasting via modular multi-task learning. IEEE Transactions on Consumer Electronics, 70(1), 1857–1865. https://doi.org/10.1109/TCE.2023.3321324

[19] Amoruso, F., & Cebon, D. (2025). Brake-actuated steering control strategy for turning of articulated vehicles. Vehicle System Dynamics, 63(2), 424–454. https://doi.org/10.1080/00423114.2024.2342535

[20] Uhlemann, N., Fent, F., & Lienkamp, M. (2024). Evaluating pedestrian trajectory prediction methods with respect to autonomous driving. IEEE Transactions on Intelligent Transportation Systems, 25(10), 13937–13946. https://doi.org/10.1109/TITS.2024.3386195

[21] Shahirpour, A., & Reuscher, T. (2025). Design and experimental evaluation of model predictive control for autonomous articulated dump trucks. Mining, Metallurgy & Exploration, 42(4), 1975–1987. https://doi.org/10.1007/s42461-025-01265-6

[22] Feng, Y., Ye, Q., Candela, E., Escribano-Macias, J. J., Hu, B., Demiris, Y., & Angeloudis, P. (2025). Risk-aware stochastic vehicle trajectory prediction with spatial-temporal interaction modeling. IEEE Open Journal of Intelligent Transportation Systems, 6, 37–48. https://doi.org/10.1109/OJITS.2025.3530268

[23] Zhang, B., Xue, F., Zhou, Y., Tian, H., & Zhang, X. (2025). A study on state estimation of distributed electric drive articulated vehicle. Journal of Computational Design and Engineering, 12(8), 286–306. https://doi.org/10.1093/jcde/qwaf066

[24] Yan, X., Feng, S., LeBlanc, D. J., Flannagan, C., & Liu, H. X. (2024). Evaluation of automated driving system safety metrics with logged vehicle trajectory data. IEEE Transactions on Intelligent Transportation Systems, 25(8), 8913–8925. https://doi.org/10.1109/TITS.2024.3397849

[25] Xu, Y., Chen, S., & Li, Q. (2026). Correcting autodifferentiation in neural ODE training. SIAM Journal on Applied Mathematics, 86(5), 2360–2378. https://doi.org/10.1137/25M172673X

[26] Celia, M., Monaco, S., & Apiletti, D. (2025). A comparative study of neural ordinary differential equations and neural operators for modeling temporal dynamics. Neural Computing and Applications, 37(30), 25319–25338. https://doi.org/10.1007/s00521-025-11580-0